Edinburgh Research Explorer

High temperature oxidation resistance in titanium-niobium alloys

OPEN ACCESS

High temperature oxidation resistance in Titanium-Niobium Alloys

B.E.Tegner [1], L.Zhu [1,2], C.Siemers [3], K.Saksl[4] and G.J. Ackland[1]∗

[1] *School of Physics, SUPA and CSEC, The University of Edinburgh, Edinburgh, EH9 3JZ, UK.*

[2] *School of Materials Science and Engineering, Beihang University, Beijing, China 100191.*

[3] *Technische Universitat Braunschweig, Institut fur Werkstoffe, Langer Kamp 8, 38106 Braunschweig, Germany.*

[4] *Slovak Academy of Sciences, Institute of Materials Research, Watsonova 47, 04353 Kosice, Slovak Republic.*

∗ *Corresponding author. gjackland@ed.ac.uk*

Highlights

The conventional explanation for oxidation resistance is disproven, an alternative presented.

A generic analytic diffusion model for oxidation resistance is presented.

We develop a class of oxidation resistant niobium-titanium alloys.

Calculation, microscopy, spectroscopy and diffraction analysis of the alloys.

The theory is verified in oxidation tests.

High temperature oxidation resistance in Titanium-Niobium Alloys

B.E.Tegner [1], L.Zhu [1,2], C.Siemers [3], K.Saksl[4] and G.J. Ackland[1]*

[1] *School of Physics, SUPA and CSEC, The University of Edinburgh, Edinburgh, EH9 3JZ, UK.*

[2] *School of Materials Science and Engineering, Beihang University, Beijing, China 100191.*

[3] *Technische Universitat Braunschweig, Institut fur Werkstoffe, Langer Kamp 8, 38106 Braunschweig, Germany.*

[4] *Slovak Academy of Sciences, Institute of Materials Research, Watsonova 47, 04353 Kosice, Slovak Republic.*

* *Corresponding author. gjackland@ed.ac.uk*

Abstract

Titanium alloys are ideally suited for use as lightweight structural materials, but their use at high temperature is severely restricted by oxidation. Niobium is known to confer oxidation-resistance, and here we disprove the normal explanation, that Nb^{5+} ions trap oxygen vacancies. Using density functional theory calculation, scanning electron microscopy (SEM) and energy dispersive spectroscopy (EDS) we show that Nb is insoluble in TiO_2. In fact, the Ti-Nb surface has three-layer structure: the oxide itself, an additional Nb-depleted zone below the oxide and a deeper sublayer of enhanced Nb. Microfocussed X-ray diffraction also demonstrates recrystallization in the Nb-depleted zone. We interpret this using a dynamical model: slow Nb-diffusion leads to the build up of a Nb-rich sublayer, which in turn blocks oxygen diffusion. Nb effects contrast with vanadium, where faster diffusion prevents the build up of equivalent structures.

Keywords: transition metal alloys and compounds; gas-solid reactions; oxidation; computer simulations; scanning electron microscopy, SEM; synchrotron radiation;

---

1. Introduction

Titanium alloys have a combination of low weight and high strength which makes them attractive for a wide range of applications[1, 2, 3]. Much of the cost of titanium stems from the difficulty in reducing the oxide to the metal[4, 5], but once purified, titanium is resistant to reoxidation on account of a thin TiO_2 layer which forms spontaneously when a clean surface is exposed to air. However, at temperatures above 600^oC, this oxidation resistance is dramatically lost. This effect prohibits the application of titanium alloys in high temperature environments, e.g. in gas turbines, for which they are otherwise very well suited.

Considerable empirical efforts have been made to improve the oxidation resistance at high-temperature of both Ti and TiAl, and the most effective of these are alloying with silicon or niobium[6, 7, 8, 9, 10]. Silicon causes the formation of a thin SiO_2-layer at the metal-oxide interface forming a diffusion barrier for oxygen. Niobium is most stable as a pentavalent ion, and it has previously been believed that the effect is due to Nb^{5+} ions in the TiO_2 surface layer; it was proposed that Nb^{5+} ions induce compensating Ti^{3+} ions which in turn trap the oxygen vacancies whose motion provides the mechanism for oxide growth.[6, 8]. Other postulated causes involve Nb_2O_5, cosegregation with Al or N, and formation of mixed oxides[7]. It is curious that Vanadium does not inhibit oxide growth, although one might expect that V^{5+} ions should play a similar role to Nb^{5+}. Furthermore, in recent calculation we have shown that a system of TiO_2 coexisting with Ti is not thermodynamically stable[11], and that the rate-limiting step in oxide growth is the production of oxygen vacancies at the metal-oxide interface[12, 13], not the diffusion in the oxide. A single-layer barrier leads to linear growth, not the $\sqrt{t}$ dependence expected for a diffusion process.[14]

To examine these issues we have performed a combination of experimental and theoretical studies on binary Ti-Nb and Ti-V alloys. The purpose of this is to uncover whether Nb is solely responsible for oxidation resistance, to study the mechanism by which it operates, and to explain why vanadium is different.

2. Methods

2.1. DFT Simulation Details

We have carried out electronic structure calculations using density functional theory using the VASP[15], code with up to 360 atoms.

The projector augmented wave (PAW) method[16], was employed to describe the electron-core interaction, with the $3p$ semicore electrons of all 3d elements being treated as valence[17]. Exchange-correlation effects were described using the spin-corrected parameterization of Perdew and Wang (PW91).[18]. These choices were compared with various alternatives[19] (Appendix), which also helps to quantify the accuracy of the theory. Ground-state atomic structures were obtained by moving atoms to reduce the Hellmann-Feynman forces, to less than 0.05eV/Å. Diffusion barriers were calculated using the nudged elastic band method, and are in agreement with previous work where it exists[20, 21]. The cutoff energy is set as 300 eV, and Gamma k-point sampling is used.

The driving force for Nb-segregation is the difference in chemical potential between oxide and the metal. This calculated using an interface structure that contains both oxide and metal[13] ($9 \times 9 \times 55$Å; 360 atoms). Specifically, it is the difference in total energy between two calculations: one with Nb substituted for a Ti atom in the metal, and one with Nb substituted for a Ti in the oxide. These two simulations have precisely the same number of each atomic species, so the atomic chemical potential is set automatically. The presence of the metal in the supercell calculations gives rise to a Fermi surface which automatically sets the chemical potential for the electrons, avoiding the complications regarding the charge state of the ions encountered for defects in ionic material.

The convergence errors of these calculations is negligible, but uncertainty of around 10% arises from the exchange-correlation functional and the choice of pseudopotential (See Appendix for details). This does not affect the central results of this paper which depend only on the fact that it is always energetically favourable to transfer Nb, V or O from the oxide into the metal.

2.2. Sample preparation

We produced seven different alloys: Commercially pure-Ti grade 2 and Ti with 0.1%, 0.5%, 1% and 2% Nb and with 1% and 2%V (formulae use weight.-%). We used ASTM-B348 Ti with 99.9% pure Nb and V. Alloys were produced by cold-hearth plasma-arc melting, doubly flushed with argon and evacuated to 5×10^{-5}mbar (3 times remelting), followed by casting into a water-cooled copper mould and stress-relief annealed at 700°C for 1 h in argon. To remove possible surface layers, moulded bars were straight-turned to a final diameter of 12mm and ground (ASTM P800) to produce a smooth finished surface for the oxidation tests. Nb and V are strong stabilizers of

the cubic β-titanium phase[6, 22], therefore, the amount of niobium and vanadium had to be limited to 2% to exclude the formation of a two-phase alloy. For sample production, the bars were sectioned into slices of 10mm length by low-speed disc cutting and again ground with P800 grinding paper. Samples were weighed by precision scales (accuracy: 0.1mg) and measured by a micrometre gauge (accuracy 0.01mm).

2.3. Oxidation

Oxidation was carried out in a standard air furnace at 800°C ± 5°C for 24, 48, 72, 96, 144 and 288 hours. Three samples of each alloy have been used for each condition. The samples were positioned in Al_2O_3 containers so that contamination of the specimens, e.g. by chemical reactions, could be neglected. In addition, it was ensured that even if parts of the oxide layer peeled off during oxidation all fragments were collected with the sample to measure the weight gain.

After weighing, all the oxidized cylinders were embedded into Epomed amorphous, glass fibre reinforced polymer by warm embedding at 180°C, 200 bar, for 10 minutes followed by water cooling, which produced excellent gap filling. About 1mm of the face was removed by grinding to remove the oxide layer and possible preexisting alpha-case. Afterwards, the sample cross sections were ground (with papers P240, P400,P600, P800, P1200, P2500), polished (9μm, 6μm, 3μm, 1μm, OPS+H_2O_2) and etched with Kroll's solution.

The microstructure and the characteristics of the oxide layer have been investigated in a ZEISS AxioImager M2m optical microscope and a Hitachi TM 3000 scanning electron microscope equipped with a Bruker Quantax 70 energy dispersive X-ray detection system. Element mapping on carbon-coated samples has been performed to locate Nb and V.

2.4. Microfocussed XRD

One sample of Ti 2Nb alloy, oxidised for 96 hours, was used in a micro-focused hard X-ray experiment at beamline P07 at PETRA III. The beam energy was 84.40 keV, resulting in a wavelength of 0.01462 nm. The sample had its polymer removed and was ground to 5 mm thickness. It was oriented as shown in Fig.5 so that the focused beam passed only through alloy or oxide,

80 diffraction patterns were taken from this sample, starting at the oxide layer towards the centre of the specimen. The area of exposure was 3 μm

x 30 μm. Each pattern overlapped with the previous by approx. 2 μm. The patterns were recorded using a Perkin Elmer 1621 detector, using ten shot averaging[23]. As a result, about 35 patterns from the oxide layer, 10 patterns from the oxide-metal-interface region and 35 patterns of the base material could be analysed. The related phases have been identified using the fit2D and CMPR software[24].

3. Theory and Calculation

To assist interpretation of our calculated and experimental results, we introduce a diffusion model to follow the dynamical growth of the surface structures.

Diffusion in the system is governed by three factors, the diffusion constant (determined by atomic migration barriers and attempt frequencies), the driving force (chemical potential) and the initial conditions. The diffusion constant for oxygen varies by many orders of magnitude between oxide and metal, and has a delta-function barrier at the interface. This is defined by the oxygen content itself and has been considered in detail in a previous paper[13].

Here we take the low concentration limit for Nb and O diffusion in the Ti bulk, with a fixed chemical potential for O at the $x = 0$ boundary, which represents the oxide interface. We assume that the migration barrier for oxygen reduced linearly with lattice spacing, so the atomic mobility varies exponentially with concentration of oxygen: the DFT calculations show that oxygen has by far the strongest effect on lattice parameter increase. The effect of this term is that in regions of high oxygen concentration, diffusion goes faster. So once a region is oxidised, the oxidisation procedes ever faster until at saturation TiO$_2$ is formed. This non-linear effect gives a mathematical description of the sharp interface between fully oxidised and unoxidised material.

Diffusion gives a net flux of element i of

$$J_i = D_i c_i / \mu_i \nabla . \mu_i$$

where the excess chemical potentials are

$$\mu_O = c_O(1 + V c_{Nb}); \qquad \mu_{Nb} = c_{Nb}(1 + V c_O)$$

and diffusion constants

$$D_O = D_1 \exp\left(1 + a_{OO} c_O\right); \qquad D_{Nb} = D_2 \exp\left(1 + a_{ONb} c_O\right)$$

6

where V is the mean repulsive energy per atom between O and Nb. The a_{ij} represent the effect on the mobility of j due to the other species i. This is primarily due to the increased lattice parameter, and since the effect of Nb is small, we approximate $a_{NbO} = a_{NbNb} = 0$.

In principle this model could be parameterized with DFT data (Table 1) for barriers and attempt frequencies. In practice, oxygen has competing diffusion pathways[25] in Ti, complicated by the solute's diffusion along dislocations and grain boundaries[26]. Furthermore, rates depend exponentially on the barrier height, such that the 0.2eV uncertainty arising from exchange-correlation and pseudopotentials translates to an order of magnitude in diffusion rate.

The exponential dependence of migration on barrier energy, and the multiple diffusion along grain boundaries, means that the ab initio energies are used as a guide only: e.g. Nb is the only element which increases all diffusion barriers[27]. Consequently, we examine the regimes of behaviour of the model rather than trying to make quantitative predictions. The regime relevant to Ti-Nb has slow migration of Nb in Ti, and strong chemical repulsion between Nb and O.

The simple model successfully reproduces the three-region structure with a growing Nb-poor region containing some O, distinct boundary to a Nb-rich region, and a gradual return to bulk concentrations. Although the model does not explicitly include microstructure, it predicts increased atomic motion in the O-rich region, which provides an explanation for the observed recrystallisation.

The model is not fitted explicitly to data, so the numerical values serve primarily to set the units of length, energy and time. The initial concentration of Nb represents the 1% alloy, while the initial concentration of oxygen, c_O, is tiny and has no effect on the results. The key features of the parameterization are the mutual repulsion between Nb and O, that Nb has a larger diffusion constant than oxygen, and that for oxygen concentrations above 0.5% diffusion is much enhanced.

4. Results

DFT shows (Table 1) that oxygen is located interstitially in Ti and increases the volume by 7.1Å per atom, compared with 1.35Å per substitutional Nb atom and a reduction of 2.47Å per substitutional V. For equal weight percentages, O increases lattice parameter by about one order of

magnitude more than Nb does, which justifies our assumption that diffusion barriers depend on oxygen concentration.

More surprisingly, DFT also shows that Nb from a dilute Ti-Nb alloy is strongly insoluble in TiO_2: excluding entropic effects, the difference in Nb chemical potential in bulk and oxide is a massive 1.42eV/atom and the equivalent value for vanadium is 1.73eV/atom. This suggests that Nb and V ions will not be present in the oxide layer, even at 800°C. Further solubility calculation of other transition metals shows that this result is consistent with trends across the group (Fig.1). We have been unable to find a relevant phase diagram, where the chemical potential for Nb is set by the alloy. Mixed oxides can be formed[28] under highly oxidised conditions, but that is not the case here.

To check this surprising result, we have performed oxidation experiments on pure Ti-Nb binary alloys, with three Ti Grade-2 commercially-pure samples (CP-Ti) and Ti-V alloys as controls. After 96h in air at 800°C, the reduced oxidation of the Nb-containing sample is clear (Fig 2), thus no additional cosegregating elements are involved: the effect is due to Nb alone and only 0.5% is required.

We have used micro-focused X-ray diffraction, EDS scans, and point analysis of the samples to determine microstructure of the Ti-Nb samples before and after the oxidation (Figs.3(a) 5 and Figs.6). The initial samples had homogeneous Nb distribution, but after 72 hours a 3-layer structure is observed. TiO_2 scale has grown and the Nb content in the scale is zero within the accuracy of the EDS method. Below the scale, a hard, so-called alpha-case material has formed, visible in the SEM and confirmed using microhardness tests. This is also Nb-depleted, O-rich, hcp-Ti. Below this alpha-case there is a region of enhanced Nb, the concentration gradually decaying away to the bulk value. By contrast, the pure Ti shows a much thicker oxide layer, and although there is increased oxygen close to the interface, there is no distinct boundary between alpha-case and matrix (see Fig.6).

Comparing the oxide-metal interfaces of the Ti-Nb and Ti-V samples after similar treatment, the three-layer structure in Ti-Nb can be discerned, whereas the Ti-V has a simple single interface and at least ten times more oxidisation (Fig.2). The EDS study showed the absence of V in the oxide layer, reverting to the bulk value from the oxide-metal interface with no alpha-case or vanadium-rich sublayer.

The microfocussed X-ray diffraction results on Ti 2Nb enables us to clearly distinguish the three-layer structure of the surface. Fig.5 shows typ-

ical patterns for each region. The Oxide layer has smooth rings showing a fine microstructure. Crystallographic indexing shows that the region consists primarily of TiO_2 rutile, with a small minority component of Ti2O3 corundum. The corundum has slightly larger lattice parameter, suggesting a small amount of Nb may be present. The second additional zone has a spotty diffraction pattern indicating a coarse texture. The spots are indexed as hcp with a lattice parameter slightly smaller than the matrix, consistent with the incorporation of oxygen and depletion of Nb. The third zone also indexes as hcp, with lattice parameter slightly larger than the matrix. Diffraction from the bulk crystal confirms that we have single phase hcp α-Ti free from Nb precipitates or Nb-rich β phase.

5. Discussion

Both experiment and calculation make it clear that the conventional mechanism for oxidation resistance is untenable, because there is no Nb in the oxide. A new theory is required. In the cases of Ti and Ti-V, the layer thickness grows *linearly* with time, not as $\sqrt{t}$ as would be expected from a diffusion process across an ever-thickening layer[14]. Migration in pure TiO_2 is faster than in Ti, while boundary migration in the fine oxide microstructure and in Ti_2O_3 may increase diffusion still further. This implies that the rate-limiting step is not the oxide layer itself, but a barrier of constant thickness - which we have identified as crossing the oxide-metal interface.

The mechanism of oxide formation in pure Ti is not an equilibrium process. The build-up of oxide is best viewed as a jamming of oxygen atoms caused by the slow diffusion across the interface. This causes the observed well-defined interface between oxide and metal, and in previous work[13] we have shown that, at such an interface, diffusion is dominated by a single high barrier for oxygen to diffuse from oxide to metal. In this model, above 600^oC, a positive feedback effect occurs to facilitate oxidization. Fast diffusion causes a drop in oxygen concentration in the oxide, and partial transformation of TiO_2 to Ti_2O_3 with increased vacancies in the oxygen sub-lattice, allowing still faster oxygen diffusion through the oxide layer and into the bulk. If the energy released by the oxidisation is allowed to raise the temperature, then at very high temperatures the model show a transition from steady oxidization to self-sustaining burning.

By contrast, Ti-Nb shows slow sublinear growth of the oxide, (fig 2), suggesting the rate-limiting step is diffusive. Further DFT calculations show

that direct short-range interactions between Nb and O in a Ti matrix are repulsive, but too weak to affect diffusion rates at low concentrations[27]. However, the solvation energy of oxygen is severely reduced by the presence of Nb. This leads to a sharp increase in oxygen chemical potential when Nb is present, making the Nb-rich region a strong barrier against O-diffusion. The chemical potential gradients and increased lattice parameter in the alpha-case material lead to a large amount of atomic motion, which is consistent with grain growth and the coarsened microstructure observed in the focussed XRD.

This casts some light on the difference between V and Nb: the smaller, lighter V atom migrates more quickly so the layer which would inhibit the oxygen penetration beyond the alpha-case does not form. The V diffusion is not instantaneous, and one might assume that V would provide some protection against very fast oxidation if there is insufficient time for it to migrate, and indeed it is a major component of most burn-resistant alloys[29].

These considerations led us to postulate the simple diffusion model described above. The model is sufficient to produce O-rich and Nb rich layers: in Fig. 4 we show the profiles of O and Nb concentration at various times, when the chemical potential for oxygen is fixed at the oxide interface ($x = 0$). The thicker line in the figure shows an oxygen and niobium concentration profile in good agreement with the EDS scan (Fig.3).

6. Conclusion

We have carried out a detailed study of oxidation resistance in Ti alloys. We have confirmed that Nb alone confers oxidation resistance, while V does not. Further, we have shown that Nb and V are not incorporated in the oxide, invalidating the existing theory for oxidation resistance. Slow migrating Nb leads to a double-layer structure, with oxygen having crossed the TiO_2-Ti boundary forming an alpha-case piling up behind a Nb-rich layer. It is this second barrier which inhibits further O-migration, due to both the increased chemical potential for O and by increasing the O-content adjacent to the TiO-Ti interface, reducing the driving force for migration of O out of the oxide. The smaller, lighter vanadium ion migrates more quickly away from the interface so cannot build the sublayer which inhibits oxidation, however it may be effective against a more rapid process such as burning.

7. Appendix

We have converged DFT calculations precisely using progressively larger k-point sampling [19] and basis set cutoff. However, two uncontrolled approximations remain: the pseudopotential and the exchange-correlation functional. To establish the accuracy of our calculations we repeated them using the local density approximation (LDA) to exchange correlation, in place generalized gradient approximation[18], and pseudopotentials generated with 3s and/or 3p electrons treated in the core [17]. Fig 7 shows these results for the solution energy (i.e. the change in energy when a oxygen is moved from the oxide to the bulk, or a Ti atom is exchanged with a Nb/V. It can be seen that the exchange correlation accuracy is about 0.1eV while the pseudopotential can have an effect around 0.3eV. In every case, the energy is large and positive, showing that the impurity is more stable in the metal, and the equilibrium concentration in the oxide is very small. These robust conclusions are used in the paper. The actual concentration ratio depends exponentially on the energy difference, and at the temperatures of interest a few tenths of eV corresponds to an order of magnitude uncertainty in concentration. Hence calculated concentrations are not used in the paper, we simply note that the concentration of Nb/V in the oxide is tiny.

References

[1] Tarselli MA. Titanium tales. Nature Chemistry 2013;5. doi:doi:10. 1038/nchem. 1656.

[2] Aimi MF, Rao MP, C. MN, Zuruzi AS, Bothman DP. High-aspect-ratio bulk micromachining of titanium. Nature Materials 2004;3:103–5. doi:doi:10. 1038/nmat1058.

[3] Hao Y, Li S, Sun B, Sui M, Yang R. Ductile titanium alloy with low poisson's ratio. Phys Rev Lett 2007;98:216405. URL: http://link.aps.org/doi/10.1103/PhysRevLett.98.216405. doi:10. 1103/PhysRevLett. 98. 216405.

[4] Flower HM. Materials science: A moving oxygen story. Nature 2000;407:305–6. doi:doi:10. 1038/35030266.

[5] Chen GZ, Fray DJ, Farthing TW. Direct electrochemical reduction of titanium dioxide to titanium in molten calcium chloride. Nature 2000;407:361–4.

[6] Lutjering G, Williams JC. Oxidation in titanium. Titanium 2007;2nd ed.

[7] Stroosnijder MF, Zheng N, Quadakkers WJ, Hofman R, Gil A, Lanza F. The effect of niobium ion implantation on the oxidation behavior of a tial-based intermetallic. Oxidation of Metals 1996;46(1-2):19–35.

[8] Chen G, Sun Z, Zhou X. Oxidation of intermetallic alloys in ti-al-nb ternary-system. Mater Sci Eng 1992;A153:597.

[9] Perez P, Haanappel VAC, Stroosnijder MF. The effect of niobium on the oxidation behavior of titanium in ar/20%o_2 atmospheres. Oxidation of Metals 2000;53(5/6):481.

[10] Perez P, Haanappel VAC, Stroosnijder MF. The effect of niobium on the oxidation behaviour of titanium in n_2/20% o_2 atmospheres. Mater Sci and Eng A 2000;284(1–2):126.

[11] Zhu L, Hu QM, Yang R, Ackland GJ. Binding of an oxide layer to a metal: The case of ti(10-10)/tio2(100). J Phys Chem C 2012;116:4224.

[12] Iddir H, Ogut S, Zapol P, Browning ND. Diffusion mechanisms of native point defects in rutile tio2: Ab initio total-energy calculations. PhysRev B 2007;75:073203–.

[13] Zhu L, Hu QM, Yang R, Ackland GJ. Atomic-scale modeling of the dynamics of titanium oxidation. J Phys Chem C 2012;116:24201.

[14] Deal BE, Grove AS. General relationship for the thermal oxidation of silicon. J Appl Phys 1965;36:3770.

[15] Kresse G, Furthmuller J. Efficient iterative schemes for ab initio total-energy calculations using a plane-wave basis set. Phys Rev B 1996;:11169.

[16] Blochl PE. Projector augmented-wave method. Phys Rev B 1994;50:17953.

[17] Tegner BE, Ackland GJ. Pseudopotential errors in titanium. Computational Mater Sci 2012;52:26.

[18] Perdew JP, Wang Y. Accurate and simple analytic representation of the electron-gas correlation-energy. Phys Rev B 1992;46:12947–54.

[19] Monkhorst HJ, Pack JD. Special points for brillouin-zone integrations. PhysRevB 1976;13:5188.

[20] Shang SL, Hector LGJ, Wang Y, Liu ZK. Anomalous energy pathway of vacancy migration and self-diffusion in hcp ti. Phys Rev B 2011;83:224104.

[21] Hu QM, Xu DS, Li D. First-principles investigations of the solute-vacancy interaction energy and its effect on the creep properties of alpha-titanium. Philos Mag A 2001;81:2809.

[22] Tegner BE, Zhu L, Ackland GJ. Relative strength of phase stabilizers in titanium alloys. Phys Rev B 2012;85:214106.

[23] Skinner LB, Benmore CJ, Parise JB. Area detector corrections for high quality synchrotron x-ray structure factor measurements. Nucl Instrum Methods Phys Res A 2012;662:61–70.

[24] Hammersley AP, Svensson SO, Hanfland M, Fitch AN, Hausermann D. Two dimensional detector software: from real detector to idealised image or two theta scan. High Pres Res 1996;14:235.

[25] Wu HH, Trinkle DR. Direct diffusion through interpenetrating networks: Oxygen in titanium. Phys Rev Lett 2011;107:045504–.

[26] Ghazisaeidi M, Trinkle D. Interaction of oxygen interstitials with lattice faults in ti. Acta Materialia 2014;76:82–6.

[27] Wu HH, Trinkle DR. Solute effect on oxygen diffusion in alpha-titanium. J Appl Phys 2013;113:223504.

[28] Fedorov NF, Mel'nikova OV, Saltykova VA, Pivovarova AP, Dib M, Strakhov VI. The nbo5-tio2 system. Russ J Inorg Chem 1989;:741.

[29] Novovic D, Aspinwall DK, Dewes RC, Voice W, Bowen P. The surface integrity of a burn resistant titanium alloy (ti-25v-15cr-2al-0.2c wt%) after high speed milling and creep feed grinding. Proc of the 10th World Conference on Titanium Hamburg, Germany, Wiley VCH 2003;.
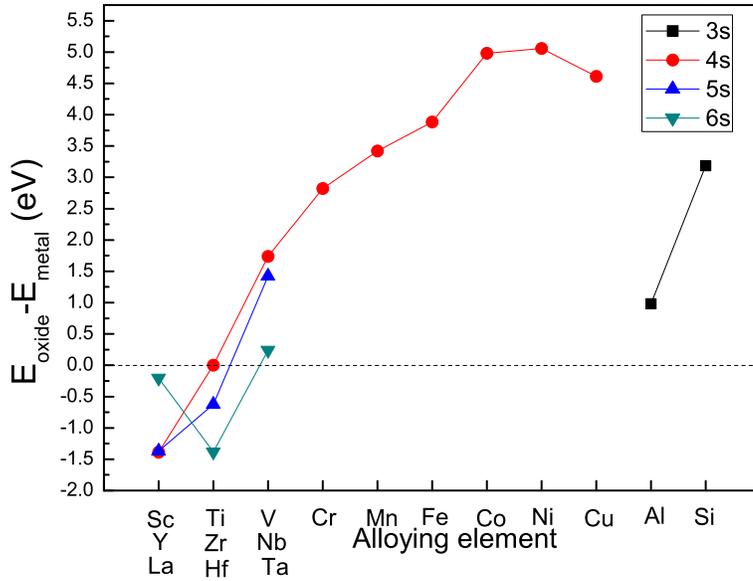
Figure 1: | **DFT results** DFT calculation for solubility of substitutional elements in TiO$_2$, compared with bulk Ti. Nb and V can be seen to be strongly insoluble, as are most other elements. This shows that whatever mechanism is responsible for the oxidation resistance conferred by Nb, it cannot occur in the oxide layer itself. Calculations show Nb has an interstitial migration barrier of only 0.51eV along [001] in TiO$_2$, while V has a more substantial 1.13eV. In metallic Ti, vacancies diffuse with barrier 0.4-0.5eV and while Nb binds vacancies by 0.15eV, V repels by 0.02eV.
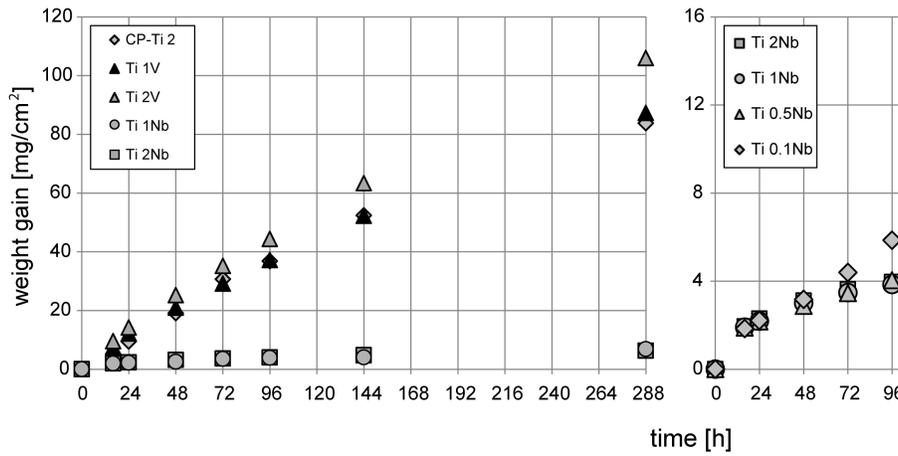
15

Figure 2: **Mass increases** due to oxidation, (left) for commercially pure Ti, and model alloys with Nb and V (by weight) respectively, after oxidation for various times at 800°C. (right) for alloys with Nb concentration from 0.1% to 2%. The figure demonstrates that even small amounts of Nb give pronounced oxidation resistance, and the effect is saturated with the addition of 0.5 wt-%.
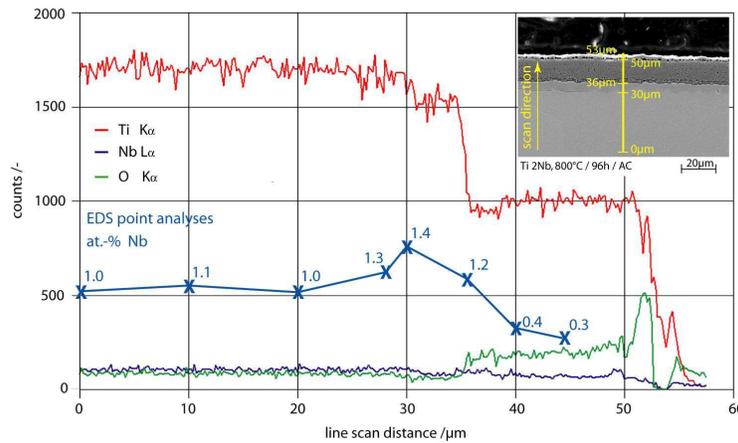

Figure 3: **Composition profiles from Energy Dispersive Spectroscopy** scans of the Ti 2%Nb sample after oxidation at 800°C for 96h and showing distinctive Nb-free oxide (shaded grey), Nb-depleted alpha-case (yellow), Nb-enriched sublayer (red) and bulk material. inset: SEM scan, with yellow line defining x-axis of main figure
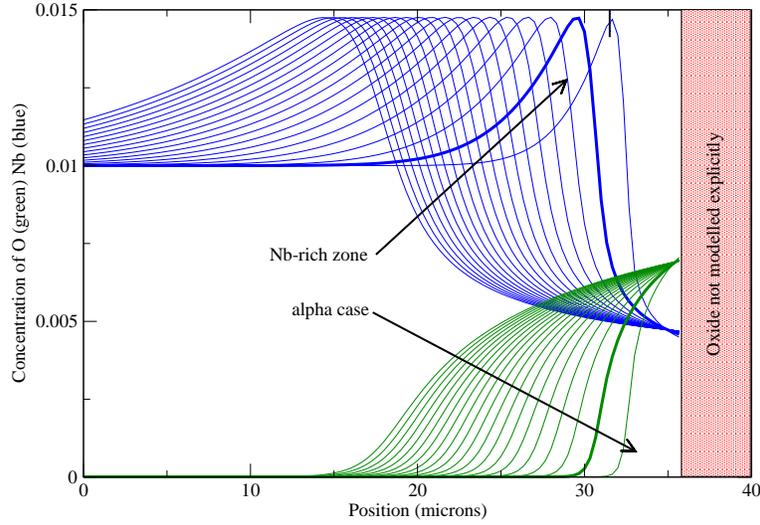
16

Figure 4: **Composition profiles from diffusion model** Successive lines are for equal time intervals from left to right, showing slower growth as they get closer. The model has not been exactly parameterized, due to the exponential dependence of the parameters on the DFT-calculated barriers so there are no units shown. Nondimensional parameters used in this figure are $V = 400$, $\mu_O(0) = 0.02$, $D_O = 0.00001 \exp(1 + 600c_O)$, $D_{Nb} = 0.0005 \exp(1 + 600c_O)$. The initial concentrations were $c_{Nb} = 0.01$, $c_O = 0.00001$, with the chemical potential for oxygen held fixed at x=0 to represent the oxide interface. and the x-axis has been scaled such that the thicker lines correspond to the EDS data in figure 3. In both figures green lines are used for O and blue lines/crosses for Nb.
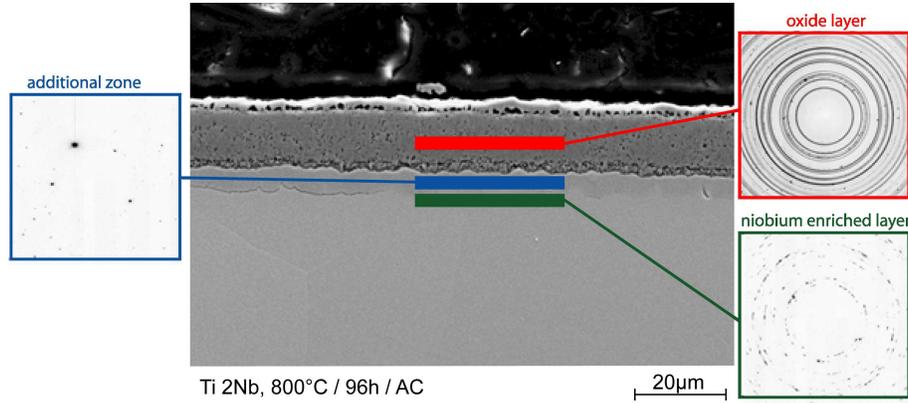
17

Figure 5: **Micro-focused hard X-ray diffraction patterns** from the Ti 2Nb sample. The beam size was 3μm x 40μm. This gives us spatially resolved phase analysis and lattice constant determination down to a depth of 100micron. The diffraction patterns shown are typical of over 100 taken, showing (red) fine grain size in the oxide, which is predominantly pure TiO_2. (blue) Large grain-size of hcp-Ti in the additional zone: Nb-depleted alpha-case region, (green) intermediate grainsize of hcp-Ti in the Nb-rich region, with lattice parameter slightly larger than the matrix.
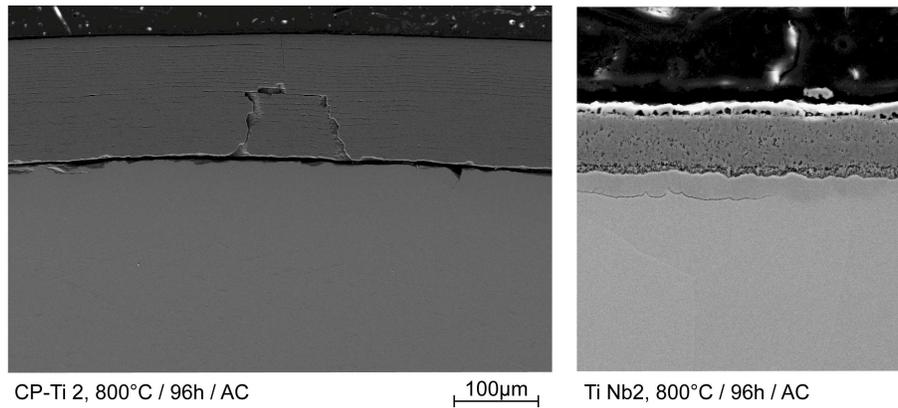

Figure 6: Cross section of CP-Ti(left) and Ti 2Nb (right) after 96 hours of oxidation at 800°C. The additional alpha-case zone in Ti 2Nb alloy at the metal-oxide-interface is clearly visible: no such feature is seen in CP-Ti or Ti-V alloys. The CP-Ti has a crack below the oxide, and the oxide itself has a multilayer structure (Ti-V alloys are similar). In Ti-Nb, the oxide layer is dense and well adhered, and there is no fracture of the surface, which has been suggested as a possible cause of linear oxide growth. [9]

18

System	Supercell energy	Volume	Binding energy
Ti	-7.763	17.50	$\mu_{Ti} = -7.763$
Ti_{53}	-409.52	ΔV_{vac}=+11.4	ΔE_{vac}=+1.92
Ti_{63}	-487.15	ΔV_{vac}=+11.2	ΔE_{vac}=+1.92
$Ti_{54}O$	-430.051	ΔV_O=+7.1	μ_O= -10.82
$Ti_{53}Nb$	-421.182	ΔV_{Nb}=+1.35	μ_{Nb}= -9.71
$Ti_{63}Nb$	-498.662	ΔV_{Nb}=+1.4	μ_{Nb}= -9.69
$Ti_{53}NbO$ (NN)	-431.766	ΔV_{Nb+O}=+9.0	$\Delta E = +0.24$
$Ti_{53}NbO$ (far)	-432.002	ΔV_{Nb+O}=+8.4	$\Delta E = +0.0$
$Ti_{62}Nb$ (NN)	-488.96		$\Delta E = +0.09$
$Ti_{62}Nb$ (far)	-488.871		$\Delta E = +0.0$
$Ti_{53}V$	-420.069	ΔV_V=-2.47	μ_V= -8.59
$Ti_{63}V$	-498.662	ΔV_V=-2.63	μ_V= -8.53
$Ti_{53}VO$ (NN)	-430.726	$\Delta V_{V+O} = +3.42$	$\Delta E = +0.15eV$
$Ti_{53}VO$ (far)	-430.832	$\Delta V_{V+O} = +3.28$	$\Delta E = +0.04eV$
$Ti_{62}V$ (NN)	-490.034		$\Delta E = +0.09$
$Ti_{62}V$ (far)	-490.90		$\Delta E = +0.0$
$Ti_{12}O_{18}$ (corundum)	-272.14	317.0	defines μ
$Ti_{11}O_{18}$+Nb	-272.16	ΔV_{Nb}=+0.02	$\Delta E = 1.833$
$Ti_{11}O_{18}$+V	-271.57	ΔV_V =-0.57	$\Delta E = 1.523$
$(TiO_2)_{84}$ $Ti_{107}Nb$	-3103.273		
$(TiO_2)_{83}NbO_2$ Ti_{108}	-3101.851		ΔE=1.42
$(TiO_2)_{84}$ $Ti_{107}V$	-3103.273		
$(TiO_2)_{83}VO_2$ Ti_{108}	-3101.851		ΔE=1.73

Table 1: Summary of DFT calculations. The chemical "formula" indicates the number of atoms in the supercell, e.g. Ti_{63} means a 64 atom cell with one atom removed to create a vacancy. Oxygen is always located in the octahedral site, Nb and V are substitutional. The 64 atom supercell is a 4x2x2 repeat of the 4-atom tetragonal hcp unit cell, while the 54 atom cell is a 3x3x3 repeat of the monoclinic 2-atom cell Supercell total energies are in eV compared to free atoms and volumes in $Å^3$/atom. Binding energies denoted by μ are used as reference energy for those denoted by ΔE. "NN" denotes nearest neighbour site, "far" denotes maximum oxygen-solute distance allowed by the supercell.
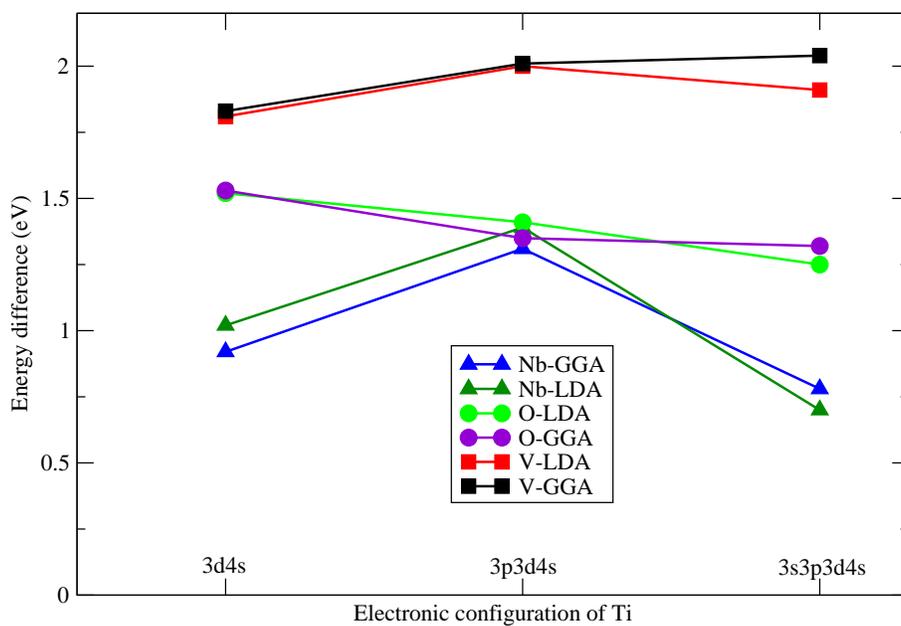
Figure 7: Sensitivity of DFT calculation of the chemical potential energy difference in metal and oxide to the choice of pseudopotential (reference configuration used to generate within PAW scheme) and exchange-correlation functional (GGA vs LDA). The positive energy seen in all cases shows a preference for the solute to be located in the metal.